JOURNAL OF SOLID STATE CHEMISTRY 105, 197–210 (1993)

An X-Ray Diffraction Study of the Oxygen Content Phase Diagram of $La_2NiO_{4+\delta}$

D. E. RICE AND D. J. BUTTREY*

Department of Chemical Engineering, University of Delaware, Newark, Delaware 19716

Received April 16, 1992; in revised form September 18, 1992; accepted November 11, 1992

The oxygen concentration phase diagram of $La_2NiO_{4+\delta}$ has been constructed from room temperature X-ray powder diffraction data on specimens spanning a wide range of oxygen stoichiometries. Contrary to some previous reports, we find multiple biphasic regions. The most stoichiometric phase ($\delta \approx 0.00$) is orthorhombic with *Bmab* (low temperature orthorhombic, LTO) symmetry in agreement with previous studies. A new distorted tetragonal phase with $P4_2/ncm$ (low temperature tetragonal, LTT) symmetry is observed for oxygen excess levels in the range $0.020 < \delta < 0.030$. Undistorted tetragonal (high temperature tetragonal, HTT) symmetry is observed for oxygen compositions from $\delta \approx 0.055$ to at least $\delta = 0.137$. An orthorhombic phase appears for $\delta \approx 0.168$. The temperature dependence of the reduction boundary has been determined; however, in contrast with the $Pr_2NiO_{4+\delta}$ system, no evidence of the oxidation boundary has been observed. The room temperature LTT phase is consistent with lower temperature observations of weak ferromagnetism associated with spin canting.

Introduction

An extensive literature on the $La_2NiO_{4+\delta}$ system has developed in recent years due to its close relationship to $La_2CuO_{4+\delta}$, the prototype of high temperature superconductors. A survey of this literature reveals that although the influence of oxygen nonstoichiometry on structure and physical properties is appreciated, the oxygen content phase diagram has not yet been convincingly established. In the present study, we have systematically examined the relationship between oxygen content and phase behavior from the stoichiometric limit to high levels of oxygen excess with the goal of obtaining a quantitative phase diagram.

Oxygen nonstoichiometry in $La_2NiO_{4+\delta}$ arises from incorporation of excess oxygen, as has been shown from single crystal density measurements (*1*). The location of the defect site in an orthorhombic specimen with a high concentration of oxygen excess has been refined from neutron powder data by Jorgensen *et al.* (*2*) as near the (0.25, 0.25, 0.25) site in the face-centered $\sqrt{2} \times \sqrt{2} \times 1$ supercell of the K_2NiF_4 structure. This is equivalent to the (0.5, 0, 0.25) defect site proposed for the undistorted body-centered tetragonal unit cell of $La_2NiO_{4+\delta}$ (*1*). This defect site is centered in the La_2O_2 "rock salt" interlayer, coordinated tetrahedrally by interpenetrated neighboring La^{3+} and apical oxygen sites (Fig. 1), and may be thought of as occurring by intercalation. These anion defects and charge compensating holes in the basal plane are energetically favored, since the intrinsic charge separation between the electropositive La_2O_2 layers and the electronegative NiO_2 sheets is thereby reduced. Excess oxygen levels as large as $\delta = 0.15$ (*3*) and $\delta = 0.18$ (*2*) have been reported from slow cooling in oxygen, and $\delta = 0.20$ (*4*) by annealing at 600 bar oxygen at 600°C. Schart-

* To whom correspondence should be addressed.

0022-4596/93 $5.00

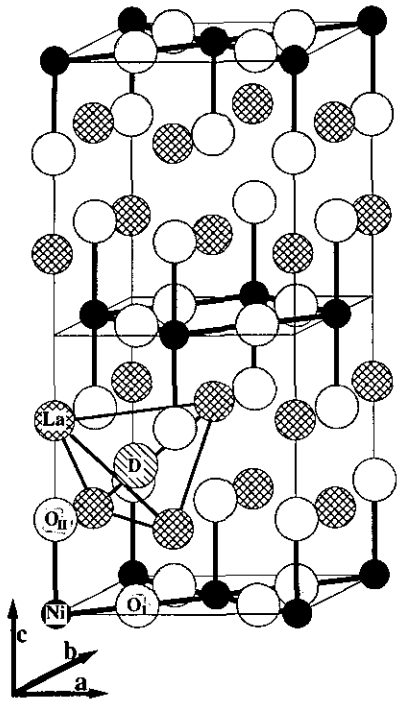

FIG. 1. The $\sqrt{2}\mathbf{a} \times \sqrt{2}\mathbf{b} \times \mathbf{c}$ $La_2NiO_{4+\delta}$ supercell without octahedral canting. The interstitial defect site (labeled "D") is shown along with an outline of the tetrahedral La-coordination environment. Note that this site is also tetrahedrally coordinated by apical oxygens (O_{II}).

man and Honig have reported thermogravimetric results on the relationship between oxygen potential and excess oxygen content, δ, at 1000, 1100, and 1200°C (*5*).

At sufficiently high temperatures La_2NiO_4 is expected to have the ideal K_2NiF_4 structure (space group *I*4/*mmm*), regardless of oxygen stoichiometry. On cooling, canting of the NiO_6 octahedra occurs as a consequence of the mismatch of geometrically constrained La–O and Ni–O bond distances. The double-degeneracy of the *X*-point of the Brillouin zone in the tetragonal high temperature structure leads to several possible symmetries which may arise on cooling by continuous phase transitions in accordance with Landau theory. This may be described in terms of an order parameter associated with octahedral canting soft modes which consists of two components, η_1 and η_2 (*6*, *7*). The Landau subgroups are all indexed on unit cells which have a doubled basal plane area relative to the parent *I*4/*mmm* structure, so that the distorted cells are larger than the undistorted K_2NiF_4 cell by $\sqrt{2}\mathbf{a} \times \sqrt{2}\mathbf{b} \times \mathbf{c}$. In comparing these structures, it is convenient to represent the undistorted structure on the expanded $\sqrt{2}\mathbf{a} \times \sqrt{2}\mathbf{b} \times \mathbf{c}$ cell also, so that the symmetry is instead described as *F*4/*mmm*. If only one of the soft modes condenses on cooling, the resulting structure is orthorhombic with space group *Bmab* [*hkl*: $h + l = 2n$; *hk*0: $h = 2n$, $k = 2n$; and *h*0*l*: $h = 2n$, $l = 2n$]. In this case the octahedra are tilted about a rotation axis parallel to **a**, the shorter of the two basal plane lattice constants. If both modes condense together ($\eta_1 = \eta_2 \neq 0$), a tetragonal structure with $P4_2/ncm$ symmetry results [*hk*0: $h + k = 2n$; and *h*0*l*: $l = 2n$]. The octahedra are tilted alternately about ⟨110⟩ and ⟨1$\bar{1}$0⟩ in neighboring layers in this case. A third possibility arises if $\eta_1 \neq \eta_2 \neq 0$, resulting in an orthorhombic structure intermediate between *Bmab* and $P4_2/ncm$ with space group *Pccn* [*hk*0: $h + k = 2n$; 0*kl*: $l = 2n$ and *h*0*l*: $l = 2n$]. It is common to refer to these symmetries as HTT (*H*igh *T*emperature *T*etragonal) for *F*4/*mmm* (or *I*4/*mmm*), LTT (*L*ow *T*emperature *T*etragonal) for $P4_2/ncm$, LTO (*L*ow *T*emperature *O*rthorhombic) for *Bmab*, and either LTO′ or LTLO (*L*ow *T*emperature *L*ess *O*rthorhombic) for *Pccn*. In some cases, an orthorhombic form is identified in which no superstructure reflections are observed, for which the symmetry appears to be *Fmmm*.

Coexisting phases in $La_2NiO_{4+\delta}$ have been reported in several investigations. In Ref. (*1*), bright-field and high-resolution imaging of a specimen which had been heated in CO_2 at 870 K revealed distinct phases in bands of light and dark contrast attributed to exsolution of a stoichiometric phase in the presence of an oxygen-excess phase. Jorgensen *et al.* (*2*), and later Rodríguez-Carvajal *et al.* (*3*), have reported observa-

tion of coexisting phases in specimens with oxygen excess levels near the midrange, $\delta = 0.07$. This phase separation behavior has been described in terms of a single miscibility gap, similar to that reported for La_2CuO_4 (*8, 9*), which separates a nearly stoichiometric composition from one with $\delta \approx 0.10$–0.13. In all of these investigations, the authors conclude that the stoichiometric phase is orthorhombic with *Bmab* symmetry, as has also been reported elsewhere (cf. *10–12*). However, in Ref. (*2*), the high δ phase is reported as orthorhombic *Fmmm*, whereas, in Ref. (*3*), the high δ phase is reported as tetragonal *F4/mmm* (HTT). The structure of $La_2NiO_{4+\delta}$ has also been described as single-phase tetragonal (*11, 12*) for preparations under conditions which are expected to produce compositions near the midrange of δ, in conflict with the proposed biphasic composition range in the oxygen content phase diagram. Furthermore, magnetic susceptibility data for low, but nonzero δ specimens, show evidence of canted antiferromagnetism with $150 \leq T_N \leq 204$ K and a net moment parallel to **c** (*13*). This observation is inconsistent with the reported spin structure of the stoichiometric *Bmab* phase and of single-phase compositions with $0.065 \leq \delta \leq 0.077$ (*11, 12*). In total, these discrepancies appear unreconcilable unless the phase diagram involves more than two phases at room temperature, or unidentified polymorphic phase transitions on cooling. Hiroi *et al.* (*4*) have reported evidence of multiple-phase separations based on TEM and X-ray data which are again inconsistent with other models for the phase diagram. The objectives of the present investigation were to systematically and quantitatively characterize the excess oxygen concentration phase diagram at room temperature.

Experimental

All specimens studied in this investigation, with the exception of two ceramically prepared samples described below, were obtained by congruent melt growth using radio frequency induction skull melting. The starting material, 99.997% La_2O_3 and 99.998% NiO, was thoroughly mixed and prereacted at 1200°C in oxidized nickel crucibles. The product was then induction melted in a water-cooled crucible in the presence of an atmosphere containing approximately 10% O_2 in CO_2. After stabilizing the melt, the crucible was lowered from within the fixed rf coil at 15 mm/hr, until coupling was lost. The resulting boule consisted of approximately 2 kg of crystals and the sintered skull. General characterization of crystals grown by this technique has been described elsewhere (*14*).

The reduction boundary was determined in the temperature range $900 \leq T \leq 1300$°C by annealing and quenching small crystals contained in a thin high-purity Ni^0 foil crucible under CO/CO_2 buffers. The relative flow rates of CO and CO_2 were adjusted with precision mass flow controllers to establish the desired oxygen fugacity, which was in turn measured electrochemically using a Y–ZrO_2 cell *in situ*. The Nernstian behavior of the electrochemical measurement was confirmed using the established Ni^0/NiO boundary and pure O_2. More than 40 anneals and quenches were performed along each of seven isotherms to locate La_2NiO_4/La_2O_3 + Ni boundary.

In order to produce specimens with various concentrations of oxygen excess, 37 groups of 5–6 crystals (totaling ~ 3 g per group) were isothermally annealed at different fixed oxygen fugacities. The majority of the anneals were carried out along the 1200°C isotherm for 8 hr or longer. Under strongly reducing conditions, CO/CO_2 buffers were employed as described above; whereas, to obtain more oxidizing conditions, O_2 diluted with CO_2 was used. All anneals along the 1200°C isotherm were monitored using the oxygen sensing cell described above. In order to achieve higher levels of oxygen excess ($\delta > 0.116$), lower temperature anneals in pure oxygen (at 1 atm) were performed. The lowest tempera-

ture anneal, 600°C, was carried out with coarsely ground material (~100 μm diameter) for over 80 days to ensure equilibration. In O^{18} diffusion studies, we have found that exchange of normal site oxygen slows rapidly below 700°C (*15*). Although we believe that equilibration of the interstitial sites occurs much more rapidly, our annealing times are conservatively based on the diffusivity data for total oxygen exchange. Following quenching, samples were immediately placed in mineral oil to avoid reaction with moisture and/or oxygen.

Two additional specimens were prepared following a ceramic synthesis similar to that described by Jorgensen *et al.* (*2*), except that we found it necessary to cycle our initial reaction at 1220°C four times with regrinding, to obtain less than 5% unreacted La_2O_3 and NiO. Following this, the sample was annealed for 4 hr at 1035°C in flowing N_2 and then furnace cooled. The sample was then partitioned, placing one portion in mineral oil and further annealing the other for 12 hr at 450°C in O_2 followed by furnace cooling and storage in mineral oil.

The concentration of excess oxygen in each specimen was determined by iodometric analysis. Titrations were carried out in an inert atmosphere glove box using deaerated solutions. Blanks showed no evidence of iodine formation. Sodium thiosulfate solutions were freshly prepared and standardized against primary As_2O_3, using concentrations appropriate for the anticipated range of oxygen contents for select groups of annealed specimens. Each iodometric analysis was carried out in triplicate, resulting in standard deviations of ± 0.002 or less (see Table I).

X-ray powder diffraction data were collected on finely ground material from each anneal using an automated $\theta/2\theta$ Philips APD3520 diffractometer equipped with a graphite monochromator on the detector arm, using CuK_α radiation. Data were collected in the range $23 \leq 2\theta \leq 97°$, using an internal (NIST) Si standard for calibration. Lattice parameters were determined by a least-squares fit to d spacings obtained from high angle data. Additional slow scans through selected ranges, such as to obtain the (200)/(020), (212), (008), and in some cases the (400)/(040) and (208)/(028) reflections, were used to characterize line profiles. This procedure was found to be particularly useful in distinguishing single and mixed phase compositions. The $\delta = 0.020(3)$ sample was further studied using synchrotron X-ray powder diffraction, carried out on beamline X7A at the National Synchrotron Light Source (NSLS) at Brookhaven National Laboratory. The ground sample was mounted on a flat plate and data were collected using a channel cut Si(111) monochromator and Ge(220) analyzer at a wavelength of 0.701046(2) Å.

Results

The reduction boundary fugacity was determined along each isotherm by the crossover from La_2NiO_4 to the reduction products, La_2O_3 and Ni(0). The resulting f_{O_2}–T relationship for this boundary is presented in Fig. 2. The boundary follows the van't Hoff dependence

$$\log_{10} f_{O_2} = \frac{-30780}{T} + 11.970,$$

where f_{O_2} is referenced to 1 atm and temperature is in Kelvins.

Iodometric data were obtained using material from each of the 37 crystalline anneals and from the two ceramic specimens. The oxygen exchange behavior and quench effects are expected to be complicated; however, all samples exhibited Bragg reflection half-widths at or near the instrument resolution limits, consistent with a homogeneous oxygen content and discrepancies between specimens from the same anneal are within experimental error. In order to produce higher levels of excess oxygen (without using superambient pressure), we carried out anneals in 1 atm oxygen at 600, 800, and 1000°C which resulted in $\delta = 0.137$, 0.122,

TABLE 1

OXYGEN CONTENT AND ROOM TEMPERATURE LATTICE PARAMETERS DETERMINED BY IODOMETRIC ANALYSIS AND X-RAY POWDER DIFFRACTION, RESPECTIVELY

δ	Space group	a	b	c	V	2c/(a + b)
0.000(1)	*Bmab*	5.4664(3)	5.5374(3)	12.5422(7)	379.65(5)	2.2796
0.007(1)	*Bmab*	5.4676(4)	5.5337(4)	12.5432(8)	379.51(5)	2.2803
0.020(2)	$P4_2/ncm$	5.4931(3)	5.4931(3)	12.5691(6)	379.26(5)	2.2882
0.030(1)	$P4_2/ncm$	5.4886(3)	5.4886(3)	12.5822(8)	379.04(5)	2.2924
0.055(2)	*F4/mmm*	5.4772(5)	5.4772(5)	12.6160(7)	378.48(5)	2.3034
0.074(2)	*F4/mmm*	5.4717(4)	5.4717(4)	12.6356(7)	378.30(5)	2.3093
0.090(2)	*F4/mmm*	5.4701(4)	5.4701(4)	12.6401(8)	378.22(5)	2.3108
0.116(2)	*F4/mmm*	5.4681(3)	5.4681(3)	12.6508(7)	378.26(5)	2.3136
0.116(2)*	*F4/mmm*	5.4656(4)	5.4656(4)	12.6567(7)	378.09(5)	2.3157
0.136(2)	*F4/mmm*	5.4619(5)	5.4619(5)	12.6799(9)	378.27(5)	2.3215
0.168(2)*	*Fmmm*	5.4664(5)	5.4653(5)	12.6932(8)	378.52(5)	2.3244

Note. Values at or very near the limits of composition for pure phases are presented in the first five rows. Results from ceramically prepared specimens are denoted by (*). Note that the $\delta = 0.000(1)$ result represents the absence of any indication of oxygen excess, but provides no information on possible oxygen deficiency (i.e., $\delta < 0$).

and 0.119, respectively. The oxidation boundary has not been observed.

Features of the phase diagram in the range $0 < \delta < 0.137$ were ascertained by examining 2θ scans from all annealed specimens through the specific reflections mentioned previously. To establish the compositional limits of each biphasic region, we studied (*i*) the pure lower δ phase near its maximum possible oxygen content, (*ii*) a biphasic mixture containing only a trace of the higher δ phase, (*iii*) a biphasic mixture with approxi-

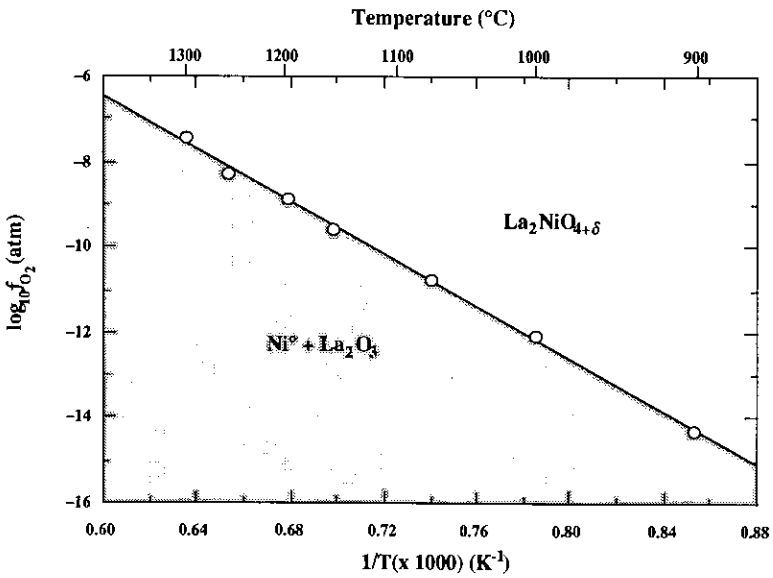

FIG. 2. The van't Hoff plot of the reduction boundary for $La_2NiO_{4+\delta}$.

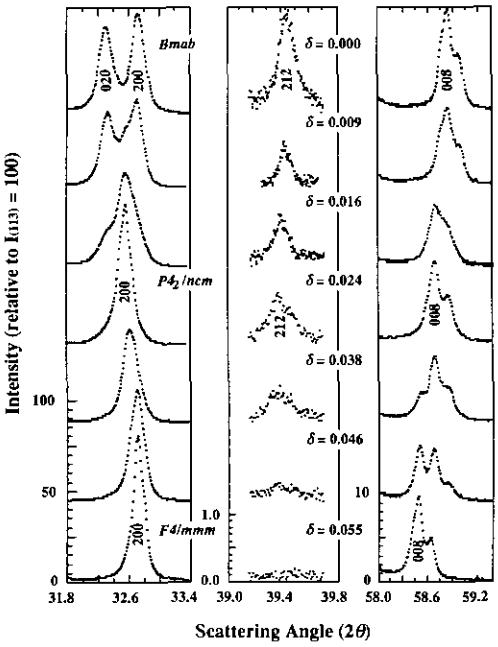

FIG. 3. A stack plot of selected Bragg reflections useful in illustrating the phase relationships with changing oxygen stoichiometry. The (212) reflection violates the face-centering general condition for *F4/mmm*, but is consistent with any of the subgroups.

mately equal amounts of both phases, (*iv*) a biphasic mixture with only a trace of the lower δ phase, and (*v*) the pure higher δ phase near its minimum oxygen content. In each case the change from two-phase to single-phase behavior was constrained to within $\Delta\delta \approx \pm 0.005$. Representative patterns obtained by sampling at 0.01° steps for 45 sec are shown in Fig. 3 along with the corresponding values of δ.

We observe single-phase patterns (*i*) near the stoichiometric limit ($\delta \leq 0.007$), (*ii*) near $\delta \approx 0.024$, and (*iii*) in the range $0.06 \leq \delta \leq 0.14$ and at $\delta = 0.168$. Initially using the fixed-source X-ray data, the observation of tetragonal or orthorhombic symmetry and the presence or absence of the (212) reflection were used to tentatively assign space groups (Fig. 4). Further evidence for these assignments was obtained from indexing more than 35 reflections from powder patterns over the full range ($23 \leq 2\theta \leq 97°$). Scans were also obtained for phase-pure compositions over the range $30 \leq 2\theta \leq 50°$ without the internal standard (Fig. 4). In each of these cases, no evidence of phase coexistence or impurity phases is visible above background, and all reflections which were expected to have measurable intensity were observed. Subsequent examination using synchrotron X-ray powder diffraction revealed trace amounts of $P4_2/ncm$ (LTT) phase in the $\delta = 0.055$ sample, which led us to set the lower δ limit of the *F4/mmm* (HTT) field at 0.058. Since $P4_2/ncm$ symmetry is normally expected far below room temperature (hence the LTT designation), we also show high-resolution synchrotron X-ray powder data as further evidence of the crystal system and conditions for allowed reflections for the $\delta = 0.020$ (sample (Fig. 5). The (200) reflection has a FWHM(2θ) = 0.013°, at or near the instrument resolution limit, confirming the tetragonal assignment. The (212) and (032) superlattice reflections, expected for $P4_2/ncm$ (but not *F4/mmm*) were clearly observed and are also shown in Fig. 5.

The lattice constants at the compositional limits were determined from biphasic specimens with compositions near the edges of the envelopes. These values were also determined for intermediate compositions within the *F4/mmm* (HTT) field as shown in Fig. 6. The lattice constants were optimized by performing at least-squares minimization based on *d* spacings obtained from the most reliable high-angle reflections. As expected, the general trend across the phase diagram is for **a** to decrease and **c** to increase with increasing δ. In the *Bmab* (LTO) phase, the magnitude of the orthorhombic strain at 295 K decreases only slightly from 1.28 to 1.20% as δ increases from 0.000 to 0.007. This subtle change is apparent in the orthorhombic splitting of (020) and (200) between the top two profiles in Fig. 4. Although the unit cell volume is observed to decrease substantially with increasing δ in the two lowest δ phases, it shows little variation over the broad HTT phase field. Based on our highest

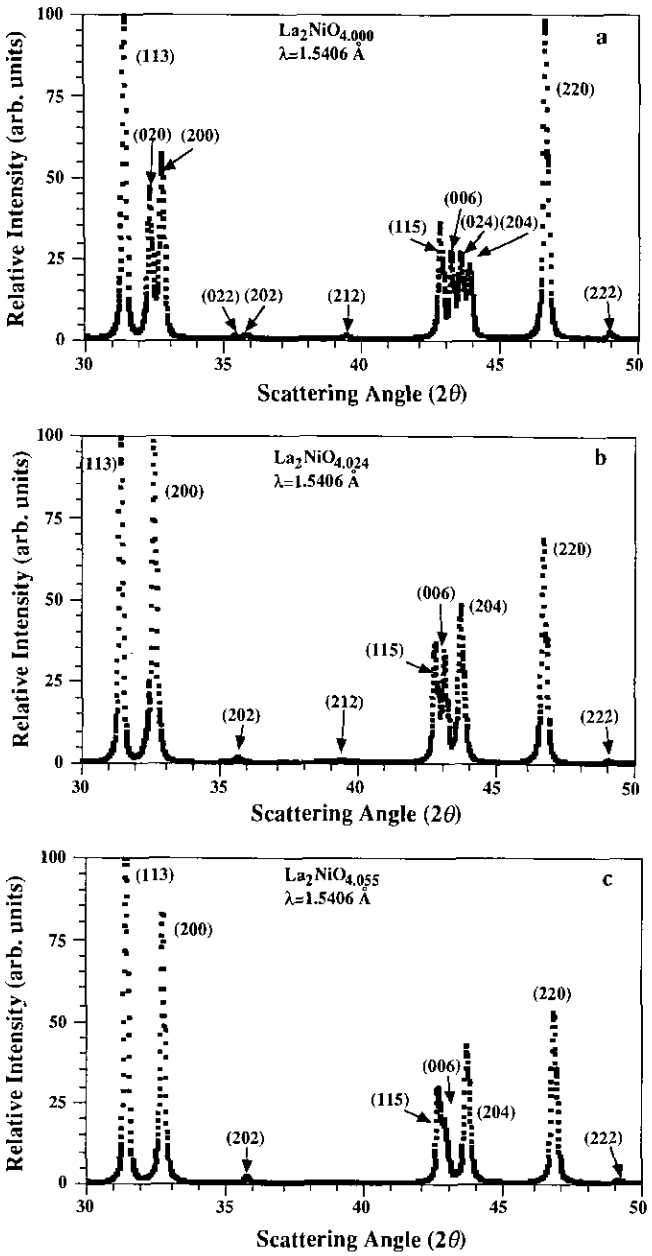

FIG. 4. Two-theta scans (fixed source, Cu$K\alpha$) in the range $30 \leq 2\theta \leq 50°$ for pure phases with (a) $\delta = 0.000$ (*Bmab* (LTO), (b) $\delta = 0.024$ ($P4_2/ncm$ (LTT), and (c) $\delta = 0.055$ (*F4/mmm* (HTT)). Note that the Si standard was omitted from these scans to avoid obstruction of the (220) profile.

δ ceramic specimen and a yet higher δ specimen described by Jorgensen *et al.* (*2*), it appears that the volume sharply increases across the highest δ phase field. We also include the variation of $2\mathbf{c}/(\mathbf{a} + \mathbf{b})$ with δ in Fig. 6d, which monotonically increases with increasing oxygen content. This is useful in comparing lattice constants from different

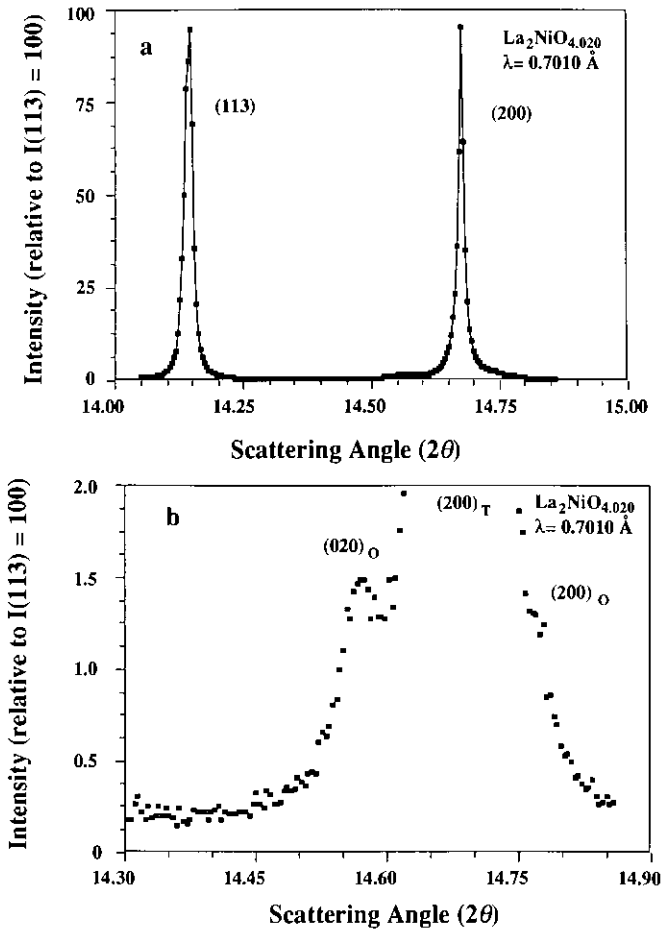

FIG. 5. Two-theta scans (NSLS synchrotron source) of the $P4_2/ncm$ (LTT) phase with $\delta = 0.020$ showing (a) the (113) and (200) with $FWHM(2\theta) = 0.013°$, (b) expanded view of the (200) reflection which reveals the (020) and (200) reflections from trace *Bmab* (LTO) phase (subscript T and O indicate tetragonal and orthorhombic, respectively), (c) (212) superlattice reflection, and (d) (032) superlattice reflection. Note that the expected locations for the corresponding *Bmab* superlattice reflections are marked by arrows, though unobserved due to the trace proportion of this phase.

diffraction studies in that it is relatively insensitive to the 2θ calibration.

Oxygen contents of $\delta = 0.116$ and 0.168 were determined for the ceramically prepared samples, the latter of which is beyond the δ range studied with the crystalline specimens. The lower δ sample exhibited lattice constants very similar to the crystalline samples with similar oxygen content and no superlattice reflections. The higher δ sample is orthorhombic with no observed superlattice reflections (space group *Fmmm*), similar to that previously reported by Jorgensen *et al.* (*2*). On the basis of these observations, we are led to believe that another biphasic region may exist at high δ (Fig. 6), probably above $\delta = 0.15$, since Rodríguez-Carvajal *et al.* (*3*) report observation of pure tetragonal phase at this composition. Patterns in the range $30 \leq 2\theta \leq 50°$ for these samples are presented in Fig. 7. The splitting of reflections in the $\delta = 0.168$ sample is difficult to resolve at low angles with conventional X-ray diffraction. Even at high angles, we

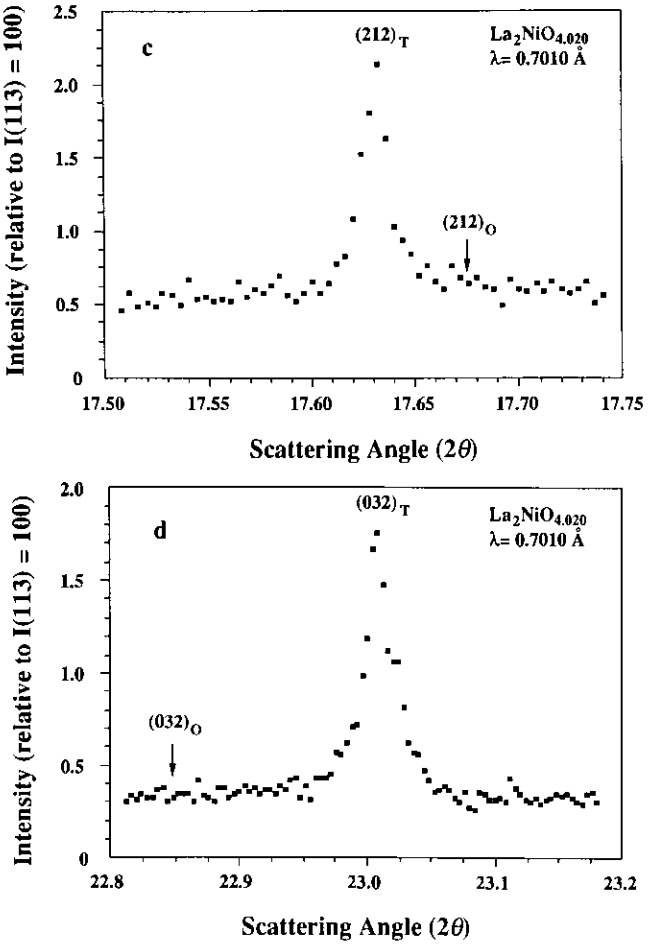

FIG. 5—*Continued*

are unable to distinguish between a monoclinic distortion of the body-centered parent cell, as was suggested by Hiroi *et al.* (*4*) for $\delta \approx 0.20$, and an orthorhombic distortion of the $\sqrt{2} \times \sqrt{2} \times 1$ cell, as suggested for $\delta \approx 0.18$ by Jorgensen *et al.* (*2*). We have chosen to index this phase on the orthorhombic cell to aid in its comparison with other compositions. High-angle data shown in Fig. 7c illustrate subtle splittings in $\delta = 0.168$ reflections, such as (513)/(153), compared with the tetragonal $\delta = 0.116$ composition. Note that the accompanying $K\alpha_2$ reflections must be considered in viewing these data and are in some cases convoluted with neighboring $K\alpha_1$ reflections.

Discussion

Hiroi *et al.* (*4*) reported TEM results showing superstructures in oxygen excess specimens, which they attribute to ordering of phases with *discreet* oxygen contents $\delta = 1/2n$, where n is an integer. While the $n = 1$ and 2 members fall outside our range of study, the $n = 3$ member is consistent with our observation of a single (orthorhombic) phase at $\delta = 0.168$, and is reasonably consistent with the report by Jorgensen *et al.* (*2*) of a similar phase at $\delta = 0.18$. The range $9 \geq n \geq 4$ spans most of our broad tetragonal range ($0.058 \leq \delta \leq 0.15$); however, we did not detect any evidence of

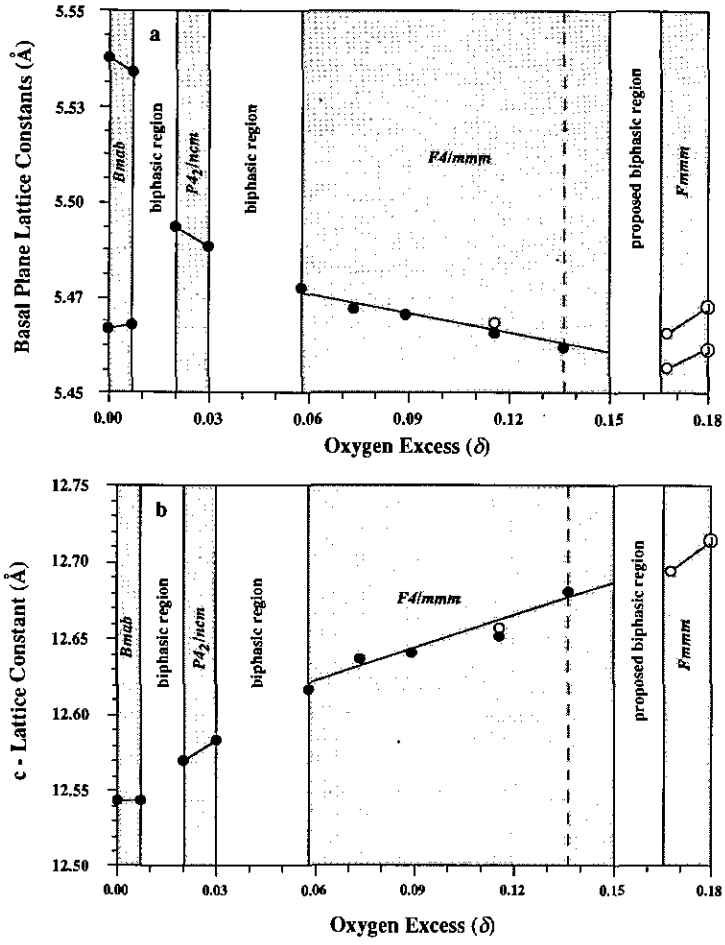

FIG. 6. Evolution of (a) the basal plane lattice constant, (b) the c-lattice constant, and (c) the unit cell volume, and (d) the 2c/(a + b) ratio (using the $\sqrt{2} \times \sqrt{2} \times 1$ cell in all cases) with oxygen stoichiometry at room temperature. The dashed line denotes the cutoff beyond which no isothermally annealed specimens were prepared. Data from our slow-cooled ceramic specimen with $\delta = 0.168$ and from results of Jorgensen *et al.* (*2*) form the basis for the proposed the high-δ biphasic region. Open circles indicate ceramically prepared samples and the open circles containing a "J" indicate the values presented in Ref. (*2*).

phase coexistence within this range at room temperature, nor did we observe any superstructure reflections. Hiroi *et al.* similarly observe tetragonal patterns in the overlapping range $0.04 \leq \delta \leq 0.12$ by X-ray diffraction. They suggest that the superstructures observed by TEM may represent short-range microstructures, arising from oxygen defect ordering, which are averaged out in X-ray and neutron diffraction measurements. Recent synchronton X-ray (*16*) and neutron scattering results (*17*) indicate that a phase separation sets in just below room temperature, leading to coexistence of tetragonal and orthorhombic phases within this midrange. In the latter study, evidence of short-range distortions is reported above the biphasic envelope. Further characterization in this composition range will be required to fully resolve the details.

In surveying the literature, it appears that there are actually only a few reports which

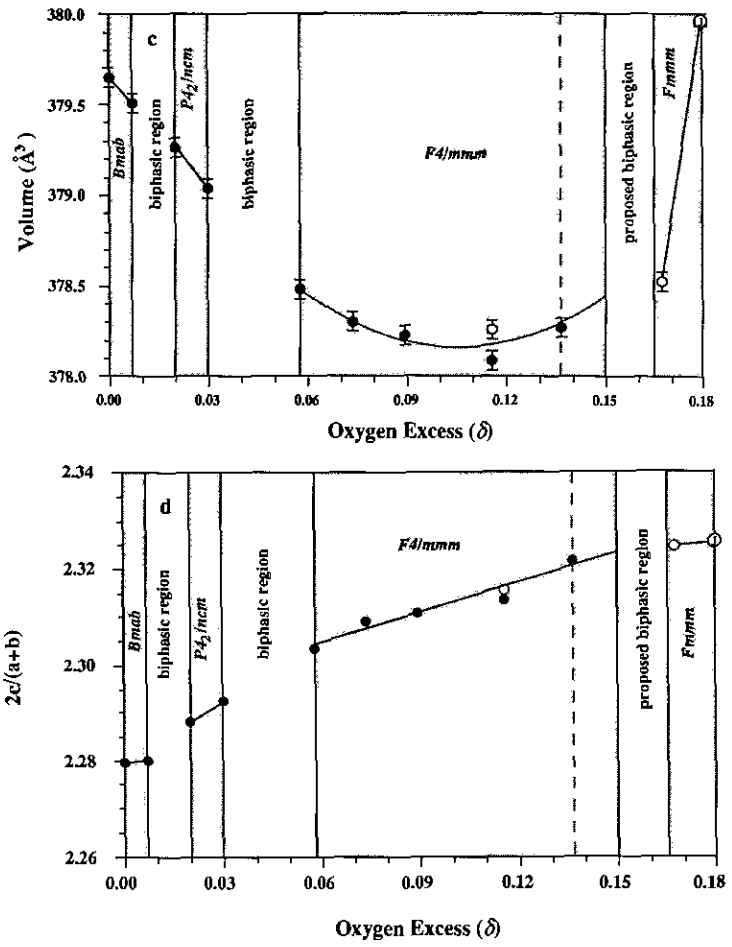

FIG. 6—*Continued*

appear to conflict with our analysis. Our results differ with those of Jorgensen *et al.* (*2*) in the midrange of composition, where they report a single biphasic region evidenced by a specimen with $\delta_{ave} \sim 0.07$. Nearly equal proportions of the two phases, each with a small orthorhombic splitting, were reported on the basis of Rietveld profile refinement of neutron diffraction data. At $T = 295$ K, the **c** parameters and 2**c**/(**a** + **b**) values, which both increase with increasing δ, are in rather close agreement with our values for the highest-δ $P4_2/ncm$ phase and the lowest-δ $F4/mmm$ phase (comparing **c** parameters of 12.5768/12.6228 Å with our 12.5822/12.6160 Å, and 2**c**/(**a** + **b**) values of 2.2905/2.3053 with our 2.2924/2.3034); however, no orthorhombic splitting was evident in our patterns and, from our analysis, an equal mix of these phases should have $\delta_{ave} \approx 0.044$. Unfortunately, our attempt to reproduce the conditions of slow cooling in N_2 used by Jorgensen *et al.* resulted in $\delta = 0.116$ rather than 0.07, apparently due to the higher residual oxygen content of our nitrogen source or a different rate of cooling.

Rodríguez-Carvajal *et al.* (*3*) also reported biphasic behavior for $\delta_{ave} \approx 0.07$. It is difficult to compare their results to our room temperature data, since the highest temperature refinement they reported for $\delta_{ave} \approx$

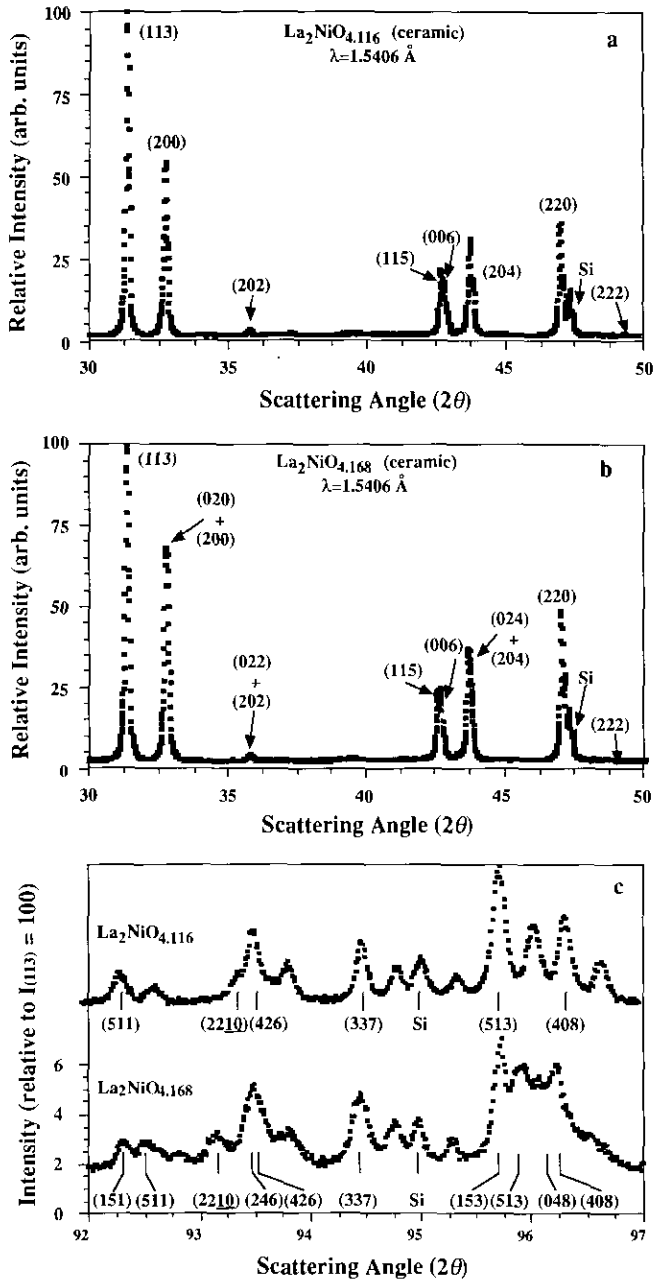

FIG. 7. Two theta scans (fixed source, Cu$K\alpha$) in the range $30 \leq 2\theta \leq 50°$ for ceramically prepared specimens with (a) $\delta = 0.116$ ($F4/mmm$ (HTT)) and (b) $\delta = 0.168$ ($Fmmm$), and (c) comparison of the high-angle reflections for $\delta = 0.116$ and $\delta = 0.168$, illustrating the slight orthorhombic splitting of the latter. Note that only Cu$K\alpha_1$ reflections are indexed and that each corresponding $K\alpha_2$ reflection occurs with roughly half intensity and ~0.30° higher in 2θ.

0.07 was carried out on data collected at $T = 180$ K; however, it is interesting to note that they observe coexistence of tetragonal and orthorhombic phases, similar to our recent low temperature results (*16, 17*). Kajitani *et al.* (*18*) reported a room temperature $P4_2/ncm$ phase with $\delta = 0.10(1)$, without evidence of a second phase; however, the expected superlattice reflections are not apparent in their X-ray patterns and the lattice constants are consistent with our findings if $\delta \approx 0.125$, which we associate with $F4/mmm$ symmetry.

The observation of a $P4_2/ncm$(LTT)-type phase at room temperature is particularly important in the context of explaining the observation of a weak ferromagnetic moment arising from spin canting at temperatures as high as ≈200 K in specimens with slight to moderate levels of excess oxygen. Spin canting is possible in the $P4_2/ncm$ and *Pccn* phases, but is symmetry forbidden in the *Bmab* phase with the established spin structure (*3, 11, 12*). Faraday measurements on an as-grown crystal of $La_2NiO_{4+\delta}$ with $\delta \approx 0.05$ showed a small cusp at the Néel point ($T_N \approx 160$ K) due to a weak ferromagnetic moment (*13*). From our phase diagram this composition should contain two phases, with the minor component (≈20%) being the $P4_2/ncm$ phase. Recent neutron scattering experiments on a crystal with $P4_2/ncm$ as the majority phase (with $\delta \approx 0.030$) indicate that $T_N = 153$ K (*17*). In the same Faraday susceptibility study, a crystal annealed at 1200°C and $\log_{10} f_{O_2}$ (atm) $= -4.6$ showed a more pronounced cusp near 200 K (*13*). Although the $[Ni^{3+}]$ was reported as approximately 0.5%, corresponding to $\delta \approx 0.010$, this appears to have been slightly underestimated. We estimate that this annealing environment should provide $\delta_{ave} \approx 0.018$ and result in a two-phase mixture with $P4_2/ncm$ as the dominant phase. In this case the $P4_2/ncm$ phase has $\delta \approx 0.020$, and we suggest that this composition will show $T_N \approx 200$ K. Subsequent reports on magnetic properties of low to moderate δ specimens frequently show $155 \leq T_N \leq 205$ K (*3, 19–21*). In a recent study by Gopalan (*19*), the dependence of T_N on δ shows plateaus at ~200 and ~155 K which we expect within the biphasic ranges bounded on the low and high δ sides, respectively, by the $P4_2/ncm$ phase.

Several common features are beginning to emerge in the oxygen content phase diagrams of the three Ln_2NiO_4 (*Ln* = La, Pr, Nd) systems. At or near the stoichiometric limit there is an orthorhombic phase with significant $(2(b - a)/(b + a) \geq 0.01)$ orthorhombic strain, having *Bmab* (or *Pccn*) symmetry at room temperature, and which undergoes a first-order phase transition in the range $60 \leq T_s \leq 120$ K to a less orthorhombic (*Pccn*) or tetragonal ($P4_2/ncm$) phase (*20–23*). As δ is increased, a phase separation region is observed in all three systems, which is bounded at room temperature by a distorted tetragonal $P4_2/ncm$ phase on the higher δ side (*22, 21, 24*). The range of δ within which this $P4_2/ncm$ phase exists is rather narrow ($\Delta\delta \leq 0.010$), at least for the *Ln* = La and Pr systems, and is centered at somewhat higher δ for *Ln* = Pr ($\delta = 0.025$ for La versus $\delta \approx 0.060$ for *Ln* = Pr) (*23, 24*). As δ is increased, additional phase separations are observed in all three systems. The higher δ phase(s) in each case shows no obvious superlattice reflections and has therefore been indexed as $F4/mmm$ (or $I4/mmm$ for the $\mathbf{1a} \times \mathbf{1b} \times \mathbf{1c}$ body-centered cell) if tetragonal and *Fmmm* if orthorhombic.

Acknowledgments

The authors gratefully acknowledge support from the National Science Foundation under Contract DMR-8914080. Synchrotron X-ray diffraction experiments were conducted in collaboration with D. Cox and J. Hriljac at the Brookhaven National Laboratories using beamline X7A at the National Synchrotron Light Source. Support for this beamline is provided by the United States Department of Energy Division of Material Sciences and Division of Chemical Sciences.

References

1. D. J. Buttrey, P. Ganguly, J. M. Honig, C. N. R. Rao, R. R. Schartman, and G. N. Subbanna, *J. Solid State Chem.* **74,** 233 (1988).

2. J. D. Jorgensen, B. Dabrowski, S. Pei, and D. G. Hinks, *Phys. Rev. B* **40,** 2187 (1989).
3. J. Rodríguez-Carvajal, M. T. Fernández-Díaz, and J. L. Martinez, *J. Phys. Condens. Matter* **3,** 3215 (1991).
4. Z. Hiroi, T. Obata, M. Takano, Y. Bando, Y. Takeda, and O. Yamamoto, *Phys. Rev. B* **41,** 11665 (1990).
5. R. R. Schartman and J. M. Honig, *Mater. Res. Bull.* **24,** 1375 (1989).
6. J. D. Axe, D. E. Cox, K. Mohanty, A. R. Moodenbaugh, and Youwen Xu, *Phys. Rev. Lett.* **62,** 2751, (1989).
7. Y. Ishibashi and I. Suzuki, *J. Phys. Soc. Jpn.* **53,** 903 (1984).
8. J. D. Jorgensen, B. Dabrowski, Shiyou Pei, D. G. Hinks, L. Solderholm, B. Morsin, J. E. Schirber, E. L. Venturini and D. S. Ginley, *Phys. Rev. B* **38,** 11337 (1988).
9. C. Chaillout, S. W. Cheong, Z. Fisk, M. S. Lehman, M. Marezio, B. Morosin, and J. E. Schirber, *Physica C* **158,** 183 (1989).
10. J. Rodríguez-Carvajal, J. L. Pannetier, and R. Saez-Puche, *Phys. Rev. B* **38,** 7148 (1988).
11. T. Freltoft, D. J. Buttrey, G. Aeppli, D. Vaknin, and G. Shirane, *Phys. Rev. B* **44,** 5046 (1991).
12. G. Aeppli and D. J. Buttrey, *Phys. Rev. Lett.* **61,** 203 (1987).
13. D. J. Buttrey, J. M. Honig, and C. N. R. Rao, *J. Solid State Chem.* **64,** 287 (1986).
14. D. J. Buttrey, H. R. Harrison, J. M. Honig, and R. R. Schartman, *J. Solid State Chem.* **54,** 407 (1984).
15. D. E. Rice, D. J. Buttrey, and W. Farneth, to be published.
16. D. E. Rice, D. J. Buttrey, J. Hriljac, and D. Cox, to be published.
17. J. M. Tranquada, D. J. Buttrey, and D. E. Rice, *Phys. Rev. Lett.* **70,** 445 (1993).
18. T. Kijitani, S. Hosoya, M. Hirabayashi, T. Fukuda, and T. Onozuka, *J. Phys. Soc. Jpn.* **58,** 3616 (1989).
19. P. Gopalan, M. W. McElfresh, Z. Kakol, J. Spatek, J. M. Honig, *Phys. Rev. B* **45,** 249 (1992).
20. D. J. Buttrey, J. D. Sullivan, G. Shirane, K. Yamada, *Phys. Rev. B* **42,** 3944 (1990).
21. J. D. Sullivan, D. J. Buttrey, D. Cox, and J. Hriljac, *J. Solid State Chem.* **94,** 337 (1991).
22. M. T. Fernández-Díaz, J. Rodríguez-Carvajal, J. L. Martínez, G. Fillion, F. Fernández, and R. Saez-Puche, *Z. Phys. B* **82,** 275 (1991).
23. J. Rodríguez-Carvajal, M. T. Fernández-Díaz, J. L. Martínez, F. Fernández, and R. Saez-Puche, *Europhys. Lett.* **11,** 261 (1990).
24. J. Allinson, S. Pudjijanto, J. D. Sullivan, and D. J. Buttrey, to be published.